Kinetics of Pearlite Spheroidization

YONG LAI TIAN and R. WAYNE KRAFT

A study of the kinetics of pearlite spheroidization under static annealing conditions was carried out in two materials—AISI 1080 steel and pure Fe-C alloy. A stereological "shape factor", F, defined as $F = S_V^p/3\overline{K}_m$, was introduced for the kinetic study. The significance of this shape factor in relation to the geometrical characters of lamellar structures is discussed. For constant temperature a linear relation between F and the logarithm of time was obtained. Analysis of the time and temperature dependencies for a constant shape factor gave an activation energy of 70 kcal/mole for AISI 1080 steel and 58 kcal/mole for Fe-C alloy which indicates that volume diffusion of Fe in ferrite is the rate-controlling mechanism. The modified fault migration theory, which was developed from the mechanism study of this research, was applied to predict the kinetics of the pearlite spheroidization. For both the AISI 1080 and the Fe-C alloy experimental results have a good match with the theoretical prediction.

I. INTRODUCTION

In reviewing the literature it became apparent that the kinetics of pearlite spheroidization has been given less than adequate attention. Only a few studies have been reported.[1–5] The difficulties arise from the complicated geometrical shapes involved during the process of spheroidization and of finding a suitable parameter to represent the shape and shape change processes. Most of the previous studies on the kinetics of pearlite spheroidization were based on the classical theory of Greenwood, Lifshitz, and Wagner (the GLW theory)[6,7,8] where microstructural features are characterized by some "local descriptors" such as mean size, $\bar{r}$, and size distribution, $f(r/\bar{r})$, which represent features of individual parts of the microstructures. These approaches gave reasonable qualitative results but often failed quantitatively. The failure may be attributed to the basic assumption of the GLW theory that the particles being measured are spherical or nearly spherical when they obviously are not in a lamellar structure. To overcome this difficulty, another parameter, the aspect ratio, has been suggested for the kinetic study of spheroidization.[2,5] The aspect ratio is indeed a good criterion to characterize the lamellar structure, because the main changes of the lamellar platelets during spheroidization are the reduction of their length and increase of their thickness which results in the decrease of the aspect ratio. However, in practice it is difficult to measure quantitatively the aspect ratio, especially when the definition as well as the measurement of the aspect ratio become ambiguous with respect to irregular shapes.

Due to the recent development of stereology, an alternative approach for the kinetic study has been developed by adopting some 'global' parameters such as specific surface area, integral mean curvature, and average mean curvature to describe morphological changes.[9] The global parameters are utilized to express the characteristics of a microstructure as a whole, or average, in terms of their linear, areal, and volume elements regardless of the local geometrical complexities. They are superior to the local parameters because they have more rigorous meaning for geometrical features without any assumption about particle size, shape, and size distribution, and they can be unambiguously measured by simple counting methods developed in quantitative microscopy. Due to these advantages, some application of global parameters to the kinetic study of recrystallization, sintering, and Ostwald coarsening have been developed,[10,11,12] but their application in spheroidization studies has been scant.

A quantitative study of the kinetics of pearlite spheroidization utilizing the global parameters is presented in this second part of our research report.[13,14] The measurements of these global parameters were accomplished by an automatic image analysis instrument and by a manual counting method. A more complex stereological parameter, called a "shape factor", is introduced. It is formed by a combination of several primary global parameters. The significance of this shape factor is discussed in terms of its relation to the geometrical features of lamellar structures during spheroidization. Finally, a quantitative analysis for the theoretical prediction of the kinetics was performed which showed a good match with the experimental results.

II. QUANTITATIVE MICROSCOPIC TECHNIQUES

Table I gives a list of symbols and definitions of the basic stereological quantities used in the present study.

Modern developments in quantitative microscopy by DeHoff,[15] Underwood,[16] and Weibel[17] have shown that the global parameters S_V, M_V, and $\overline{K}_m$ can be easily measured by simple counting methods. The relevant formulae for the interrelations between the global parameters and counting quantities are listed below.

$$V_V = A_A = P_P \quad [1]$$

$$S_V = 2N_L \quad [2]$$

$$S_V^p = 2N_L/P_p \quad [3]$$

$$M_V = 2\pi N_A \quad [4]$$

$$\overline{K}_m = M_V/S_V = \pi N_A/N_L. \quad [5]$$

In the present study, point counting and linear intercept counting were accomplished by both an automatic image

YONG LAI TIAN is Postdoctoral Fellow, Department of Materials Science and Engineering, Northwestern University, Evanston, IL 60201. R. WAYNE KRAFT is Professor, Department of Materials Science and Engineering, Lehigh University, Whitaker Laboratory #5, Bethlehem, PA 18015.

Manuscript submitted July 11, 1986.

Table I. List of Basic Stereological Symbols and Definitions

Symbol	Definition
p_p	Point fraction, number of points per test points
A_A	Area fraction, area of features per unit test area
V_V	Volume fraction, volume of features per unit test volume
N_L	Number of features intersected per unit test line
N_A	Number of features intersected per unit test area
λ_2	Mean intercept length of planar figures
S_V	Specific surface area
S_V^P	Specific surface area of components P, $(S_V^P = S_V/V_V)$
M_v	Integral mean curvature
$\overline{K}_m$	Average mean curvature

analysis instrument and by manual counting methods. Specimens with coarse interlamellar spacing were measured by a computer assisted image analyzer, the Leitz T.A.S. For specimens with fine interlamellar spacing, a manual counting method was adopted because the resolution of the Leitz T.A.S. was limited by its image input device—an optical microscope.

High contrast and high polishing quality are required for the specimens in Leitz T.A.S. measurements. Specimens were first etched in a boiling alkaline sodium picrate solution for 20 to 30 minutes (NaOH 25 mg, picric acid 2 mg, distilled water 100 ml). Cementite particles were stained to a dark black which appear in high contrast to the ferrite matrix. Measurements of point counting and intercept counting were performed by the computer *via* a predesigned program. About 60 fields were measured and the average value taken as representative of each specimen.

Specimens for manual counting were etched in 2 pct nital for a couple of seconds. For specimens with relatively coarse interlamellar spacing, manual counting was carried out on the projection screen of an Olympus optical microscope. For those with very fine microstructure, measurements were done on photomicrographs taken on an ETEC scanning electron microscope. A special transparent counting grid, as shown in Figure 1, was overlaid on the screen or pictures to facilitate manual counting. The intercepts of the microstructural features with the test points or lines were manually counted. For those features which intersect the edges of the test area a rule for counting suggested by Gundersen[18] and Weibel[17] was followed to eliminate 'edge effect'. The counting grid adopted here is the 'isotropic currilinen test system' proposed by Mertz.[19] The test lines are semicircles which overcome the difficulties caused by the anisotropy of lamellar structures. At least 20 randomly selected fields were counted for each specimen and the average value taken as the final measurement of the specimen.

III. STEREOLOGICAL MEASUREMENTS ON KINETICS OF PEARLITE SPHEROIDIZATION

A. *Principles for the Selection of a Stereological Shape Factor*

Since spheroidization of lamellar structures is a process of shape evolution of microstructures, the first step is to select

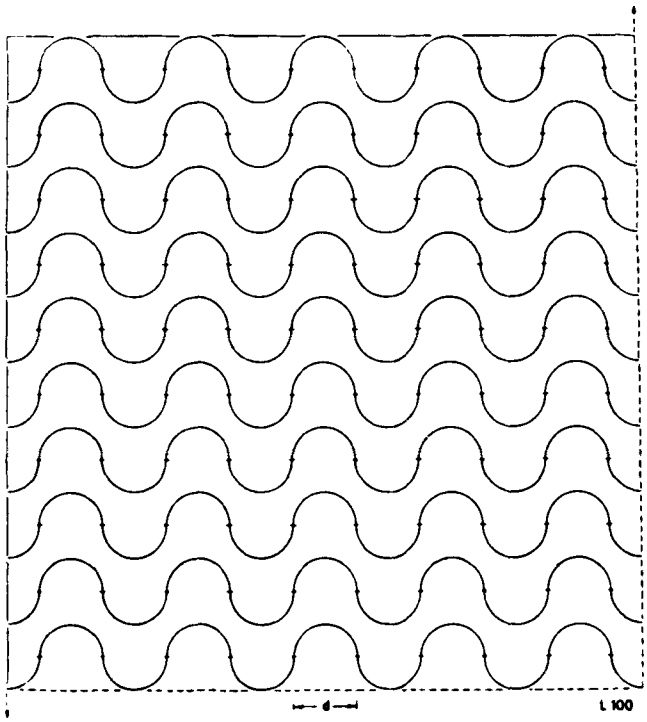

Fig. 1—Isotropic currilinen test system for manual counting.[17]

suitable criteria to evaluate shape changes. However, the quantitative expression of the shapes of microstructural features turns out to be one of the most difficult subjects in quantitative stereology. Neither a general rule nor a universally accepted criterion is available for quantitative shape evaluation. At the present stage of development of quantitative microscopy, stereologists suggest using a parameter called a 'shape factor' for an approximate expression of the shape of the microstructural features. The shape factor is usually formed by a combination of several primary stereological parameters such that it can quantitatively express the shape of the microstructural features. A variety of shape factors have been reported in the literature. The selection of an appropriate one depends on the system of microstructural features being studied and the purpose of the research. The general principles for selecting a suitable shape factor can be summarized as follows. The parameter should be (1) dimensionless; that is, it should be purely shape dependent, which is to say unaffected by absolute volume fraction, particle size, or size distribution in the system; (2) sensitive to shape change, so that the parameter reflects clearly observable shape changes; and (3) related to primary stereological parameters which can be unambiguously measured by simple counting methods.

Four classes of shape factors were summarized by Underwood,[20,21] one of which, the class 1, appears to be an appropriate one for our purpose. This shape factor was first developed by DeHoff,[22] and later on Fishmeister[23,24] modified it by changing the constant to make $F = 1$ for a spherical shape. The definition of the shape factor F given by Fishmeister is

$$F = S_V^p/3\overline{K}_m = 2N_L^2/3\pi V_V N_A. \quad [6]$$

Underwood[20,21] and Gallo[25] also recommended it as a powerful criterion to express quantitatively the shape of

microstructural features. Unfortunately, no experimental measurements using this shape factor F in microstructure or morphology studies were found in the literature. Nevertheless, this shape factor was adopted to express quantitatively the shape changes of the lamellar structure in this study.

B. *Significance of Shape Factor F in Relation to the Geometrical Characteristics of Lamellar Structures*

The shape factor F adopted here satisfies conditions 1 and 3 mentioned above because F is dimensionless and consists of primary stereological parameters. (But see Note Added in Proof.) To assess condition 2 expressions of F for three major geometrical features involved in spheroidization, *i.e.*, spheres, platelets, and rods, are derived as follows:

(1) Expression of F for a spherical shape

(r is the radius of the sphere)

$$S_V^p = 3/r,$$

$$\overline{K}_m = 1/r,$$

$$F = S_V/3\overline{K}_m = 1 \qquad [7]$$

(2) Expression of F for single cylinder or platelet

(r is the radius, x is the size, $x = 2r$, and λ is the thickness. Note that λ, the thickness, is not the same as λ_2, mean intercept length defined in Table I.)

$$S_V^p = \frac{2(1 + \lambda/r)}{(\lambda/r)r},$$

$$\overline{K}_m = \frac{\lambda + \pi r}{2(1 + \lambda/r)r^2},$$

$$F = \frac{4(1 + \lambda/r)^2}{3(\lambda/r)(\lambda/r + \pi)}. \qquad [8]$$

When $r \gg \lambda$, *i.e.*, the platelet shape,

$$F = \frac{4r}{3\pi\lambda} = \frac{2x}{3\pi\lambda} \qquad [9]$$

and when $r \ll \lambda$, *i.e.*, the cylindrical shape,

$$F = \frac{4}{3} \approx 1.33. \qquad [10]$$

The relationship between the shape factor F and the aspect ratio x/λ is calculated from Eq. [8] and is plotted in Figure 2. It is noted that when $x \gg \lambda$, *i.e.*, the platelet shape, the shape factor is linearly proportional to the aspect ratio x/λ, which means that F is indeed sensitive to changes of platelet shape. Since the majority of the geometrical features of cementite during the main process of spheroidization are the platelets, it is reasonable to believe that the shape factor F introduced here is an appropriate criterion to characterize the shape change of lamellar structures during spheroidization.

It is also seen from Figure 2 that the shape factor F becomes nearly constant at a value of 1.33 when x/λ is less than 1, *i.e.*, within the aspect ratio range of the cylindrical rods. This value is very close to that of the spherical shape ($F = 1$). Hence we know that F is not very sensitive to the shape change from a long cylinder to a short cylinder or

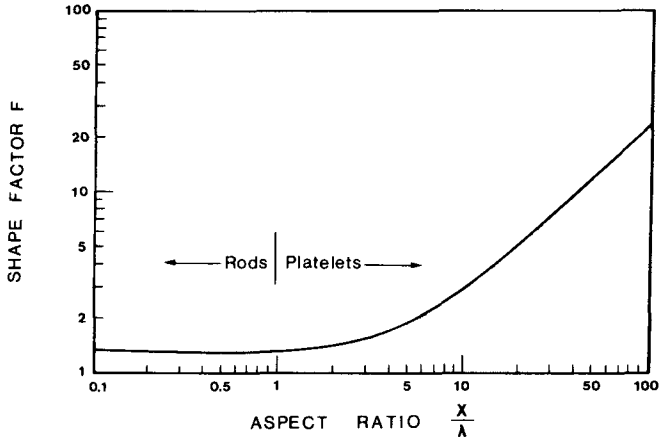

Fig. 2—The relationship between F and x/λ calculated from Eq. [8].

from a cylinder to a sphere. However, this insensitivity will have little influence on the quantitative evaluation of the shape change since the break-up of cylindrical shapes contributes only a small portion of the morphological change during the later stage spheroidization.[13]

The discussion above deals only with the expressions for a microstructure of monodispersed shape, *i.e.*, only for a single particle in the shape of a platelet or cylinder. For a real pearlitic lamellar structure, which always consists of a dispersion of various cementite platelets, the situation becomes more complicated. An explicit expression, analogous to Eq. [8], between the shape factor F and some geometrical parameters is difficult to derive since the distribution of the sizes and the aspect ratios of different lamellar platelets must be taken into account. To avoid this problem we introduce a special stereological formula given by DeHoff from his study of the stereological properties of platelet features:[26]

$$\lambda_2 = \frac{\pi^2}{4\overline{K}_m}. \qquad [11]$$

Since the mean intercept length in the plane of the platelets, λ_2, equals the average length of lamellar plates on a polished section, $\overline{x}$, we have:

$$\lambda_2 = \overline{x}. \qquad [12]$$

For an ideal lamellar structure the specific surface area, S_V, is related to the thickness of the platelets, $\overline{\lambda}$, by

$$S_V = 2V_V/\overline{\lambda}. \qquad [13]$$

Combining Eq. [6] with Eq. [11] to Eq. [13] yields

$$F = \frac{8\overline{x}}{3\pi^2\overline{\lambda}}. \qquad [14]$$

The shape factor of a single platelet (Eq. [9]) is similar to that for a lamellar structure (Eq. [14]) except for a difference in the constants. From these formulae it is clear that the shape factor represents the average value of the aspect ratio of the platelets of the lamellar structure.

C. *Stereological Measurements of Shape Factor as a Function of Time and Temperature*

In the present study the shape factor F is used as a criterion to describe the kinetics of spheroidization. The global

parameters S_V and M_V were determined by intercept counting and loops counting based on Eq. [2] and Eq. [4], respectively. The stereological measurements of N_L and N_A were carried out by either manual or automatic computer assisted measurements. The average mean curvature $\overline{K}_m$ was determined by the ratio of M_V/S_V. The results of stereological measurements for the time dependence of the shape factor F under different temperatures are plotted in Figure 3 to Figure 6. It is seen from all of these figures that for a constant temperature, F is a linear function of logarithm of time. It can be written in general as

$$F = A + b \log(t). \qquad [15]$$

The solid lines through the experimental points were drawn by a computer program of least square regression. Qualitatively, the decrease of the shape factor F as time increases can be easily understood by its geometrical meaning in relation to the average aspect ratio $\overline{x}/\overline{\lambda}$. It is known from the fault migration model that during spheroidization, the average length of the cementite platelet decreases while the thickness of the platelets increases. The overall average aspect ratio thus decreases and so does the shape factor F.

It is interesting to note from Figure 5 and Figure 6 (Fe-C alloy) that at 700 °C and at longer annealing times ($t >$ 300 hours), the F values deviate from the linear relation of Eq. [15] and tend to become constant, at a value approaching 1. Such a change in slope indicates (1) that the shape factor F is not sensitive to the shape change from cylinder to sphere (from $F = 1.33$ to $F = 1.0$); and (2) that most of the cementite particles are close to the final spherical shape. The value of $F = 1$ corresponds to the condition of the final equilibrium shape of all spheroids and no further shape evolution at all.

The simple relationship between time and shape factor F shown in Eq. [15] indicates that the shape factor is a useful criterion to describe the kinetics of the shape change of the lamellar structures. It is conceivable, from the results presented in Figure 3 to Figure 6, that there is a general relationship among the shape factor, time, temperature, and interlamellar spacing for a given material. Attempts were made in this study to establish such a general relationship, but were not successful.

Note Added in Proof

A reviewer raised interesting questions about our treatment of the shape factor which we address here.

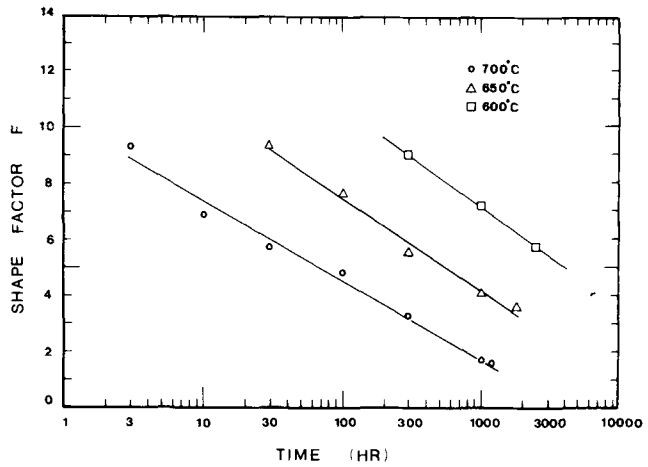

Fig 3—Plot of F *vs* log t for coarse AISI 1080 steel.

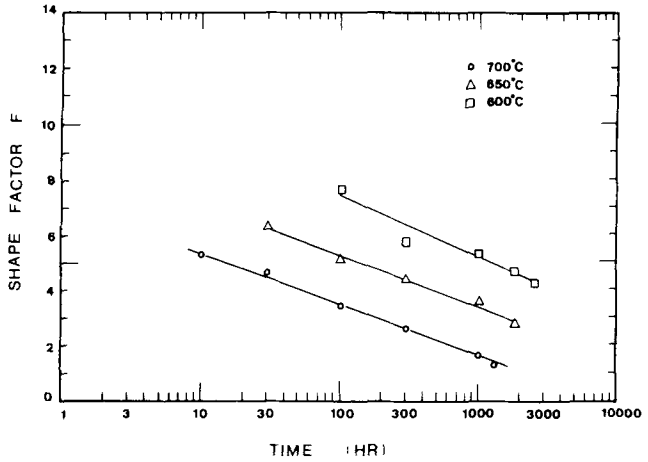

Fig. 4—Plot of F *vs* log t for fine AISI 1080 steel.

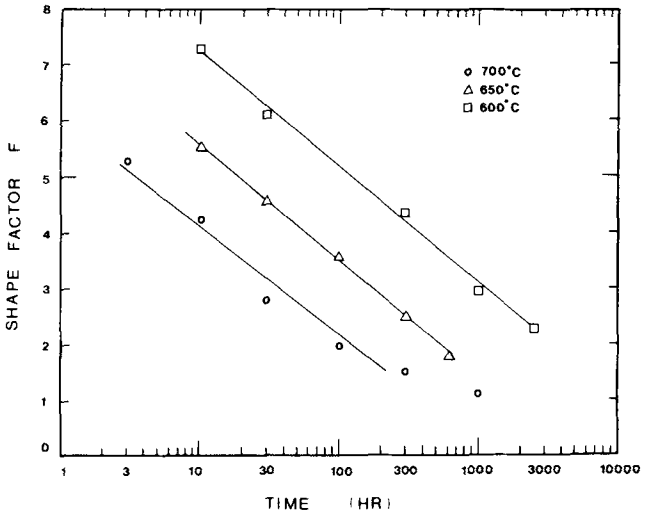

Fig. 5—Plot of F *vs* log t for coarse Fe-C alloy.

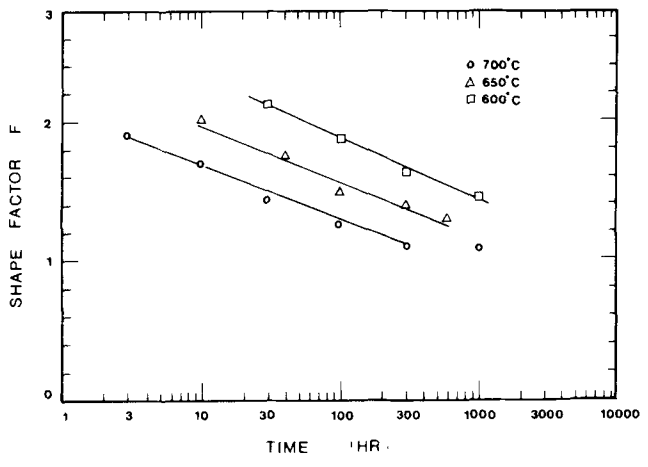

Fig. 6—Plot of F *vs* log t for fine Fe-C alloy

The basic global parameters such as S_V and M_V are fundamental in that they are independent of the size and shape of microstructural features. In contrast the shape factors are, in general, size and shape dependent. For the purpose of quantitatively evaluating a process whose essential feature is a

shape change (as is the case here), any single one of the global parameters is clearly inappropriate — because they are not shape dependent. Furthermore, the global parameters S_V and M_V would vary with sphere size in a completely spheroidized structure; that is, they would vary as Ostwald ripening occurred.

We wanted a parameter that was dimensionless (not true of S_V and M_V, but true of our F) and that was dependent only on shape. As the reviewer pointed out, no parameter that satisfies the second criterion is known: the F factor we adopted depends on shape *and size* of the particles. Hence our use of F to characterize shape change is not a "pure" measure of shape change.

However, the theory presented here shows that the dimensionless shape factor we adopted does approach a constant value (of 1) as spheroidization approaches completion and that it does not change with Ostwald ripening. Furthermore, our experimental evidence confirms that the theory is a metallurgically useful means for characterizing the spheroidization process. In addition, the F factor we adopted has a visualizable geometric meaning: it is directly related to the average aspect ratio observed on a polished microspecimen, which is the usual metallurgical criterion for evaluating degree of spheroidization.

The principal theoretical problem is establishing how much a size distribution affects the value of the shape factor. The mathematical treatment of this problem is very difficult. We circumvented this problem by introducing Eq. [11] and by noting that Eqs. [9] and [14] differ principally in the values of the constants. We conclude that the shape factor we adopted appears to be independent of the distribution of $\bar{x}/\bar{\lambda}$. However, as pointed out by the reviewer, the usefulness of this approach might be limited.

D. *Significance of Shape Factor F in Relation to the Diffusion Rate Controlling Mechanism of Pearlite Spheroidization*

Holloman and Jaffe[27] and Larson and Miller[28] investigated time and temperature effects on the properties of steel. They all made the basic assumption that the relation between time and temperature and the property they were measuring took the usual form of the diffusion equation; *i.e.*, the property is a function of the parameter $t[\exp(-Q/RT)]$:

$$P = f(t[\exp(-Q/RT)]) \qquad [16]$$

where P is some property of the material such as the hardness or strength. Q is assumed to be the activation energy for the rate controlling process. Since the property of a material is usually assumed to be related to the microstructure, it is reasonable to assume that the shape factor, F, which represents the geometrical characters of the microstructure, is also a function of the property, namely:

$$F = f'(P) = f''(t[\exp(-Q/RT)]) .$$

For a constant F, it can be shown that

$$\frac{1}{t} = A'' \exp(-Q/RT) , \quad \text{or} \quad \log t = A' + \frac{Q}{RT} . \qquad [17]$$

This is a well-known general rate equation, where A' is a constant. The computed results of $\log t$ *vs* $1/T$ for several values of F are plotted in Figure 7 to Figure 10. On these figures the points are the calculated data and the solid lines through them are computed by a least square regression. It is obvious from these figures that the linear relation of the general rate equation, Eq. [17], is followed in all cases to a very good approximation. From the slopes an average value of the activation energy of the rate controlling mechanism Q can be evaluated. The computed values of Q and A' for different materials and different interlamellar spacing are listed in Table II. The error ranges were estimated by taking the maximum deviation of each slope from the average value.

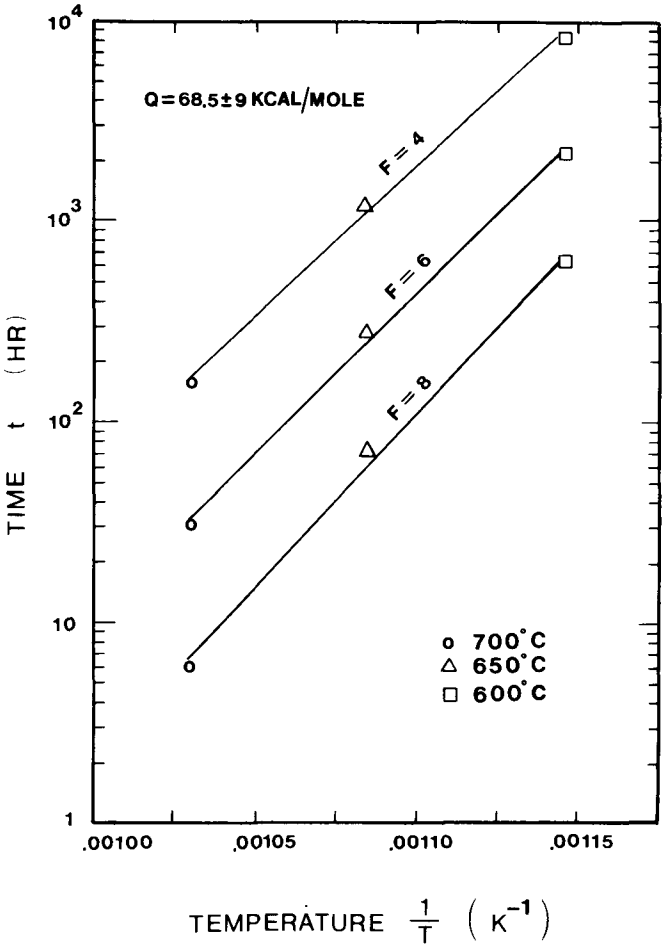

Fig. 7 — Plot of $\log t$ *vs* $1/T$ for coarse AISI 1080 steel

From these figures, it is found that the slopes for the same material are nearly constant regardless of different interlamellar spacings. This result is consistent with theory because the activation energy for diffusion depends only on the composition of the material, not on the interlamellar spacing.

The activation energy calculated from the slopes for AISI 1080 steel are about 70 Kcal/mole and for the Fe-C alloy about 58 Kcal/mole, respectively. The difference in the activation energy between AISI 1080 steel and pure Fe-C alloy may be attributed to Mn, which raises the activation energy of AISI 1080 steel. Published data for the activation energy of different diffusion mechanisms for eutectoid steels are listed in Table III.[29–33] From a comparison of our measured Q values with these data, it is concluded that for both AISI 1080 steel and Fe-C alloy the predominant rate

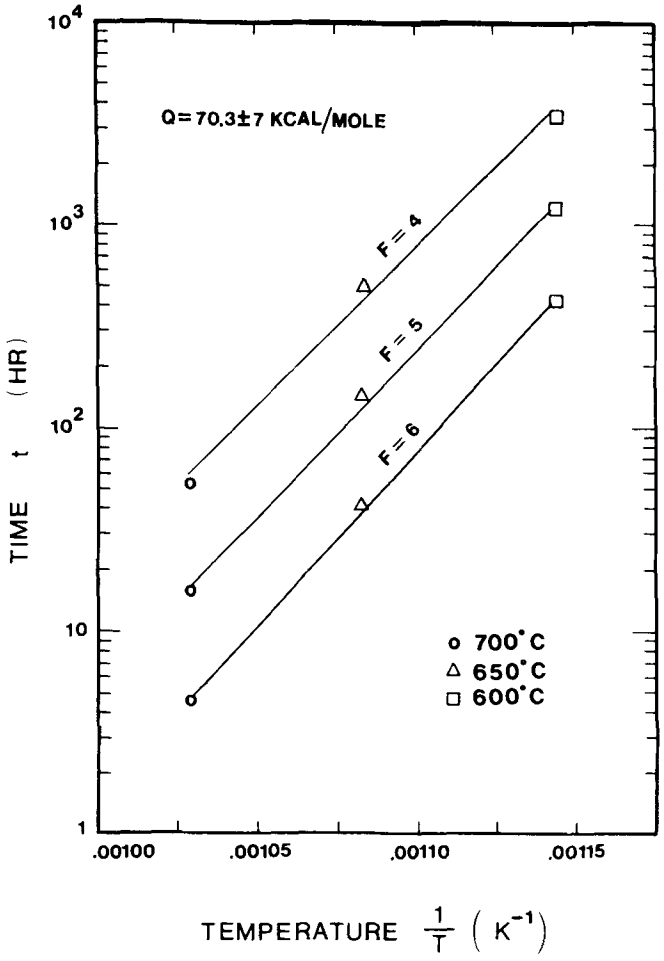

Fig. 8—Plot of log t *vs* $1/T$ for fine AISI 1080 steel.

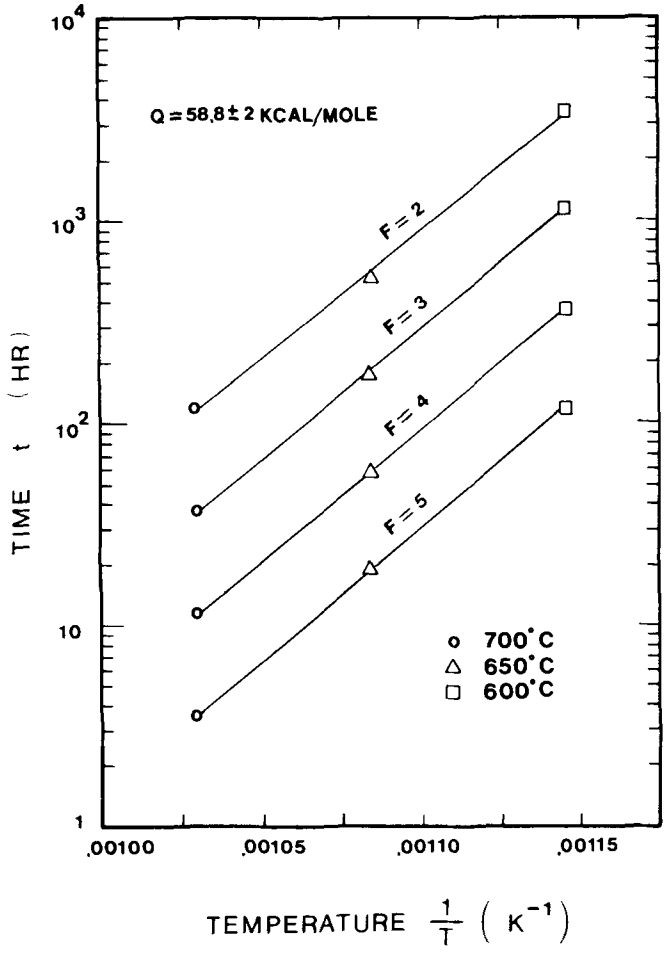

Fig. 9—Plot of log t *vs* $1/T$ for coarse Fe-C alloy.

Table II-A. Values of Q and A in Equation [17] Computed by Least Square Regression

Material	Interlamellar Spacing	Computed Constants in Eq. [17]	Shape Factor F 2	3	4	5	6	8	Average (Q/R)	Q kcal/mole
AISI 1080 steel	coarse	A'	−24.9	−27.2	−29.4	−31.6	−33.8	−38.3	34.5	68.5 ± 9
		$Q/R \times 10^3$	30.8	32.2	33.5	34.9	36.3	39.1		
	fine	A'	−26.3	−29.3	−32.3	−35.3	−38.3	—	35.4	70.3 ± 7
		$Q/R \times 10^3$	31.9	33.7	35.4	37.1	38.8	—		
Fe-C alloy	coarse	A'	−24.8	−26.1	−28.0	−29.6	−31.3	—	29.6	58.8 ± 2
		$Q/R \times 10^3$	28.7	29.2	29.6	30.0	30.5	—		

Table II-B. Values of Q and A in Equation [17] Computed by Least Square Regression (Fine Interlamellar Spacing of Fe-C)

Material	Computed Constants in Eq. [17]	Shape Factor F 1.2	1.5	1.8	2.0	2.5	Average Q/R	Q kcal/mole
Fe-C	A'	−21.0	−24.2	−27.6	−29.8	−35.3	28.4	56.5 ± 7
Fine interlamellar spacing	$Q/R \times 10^3$	25.3	26.9	28.4	29.5	32.1		

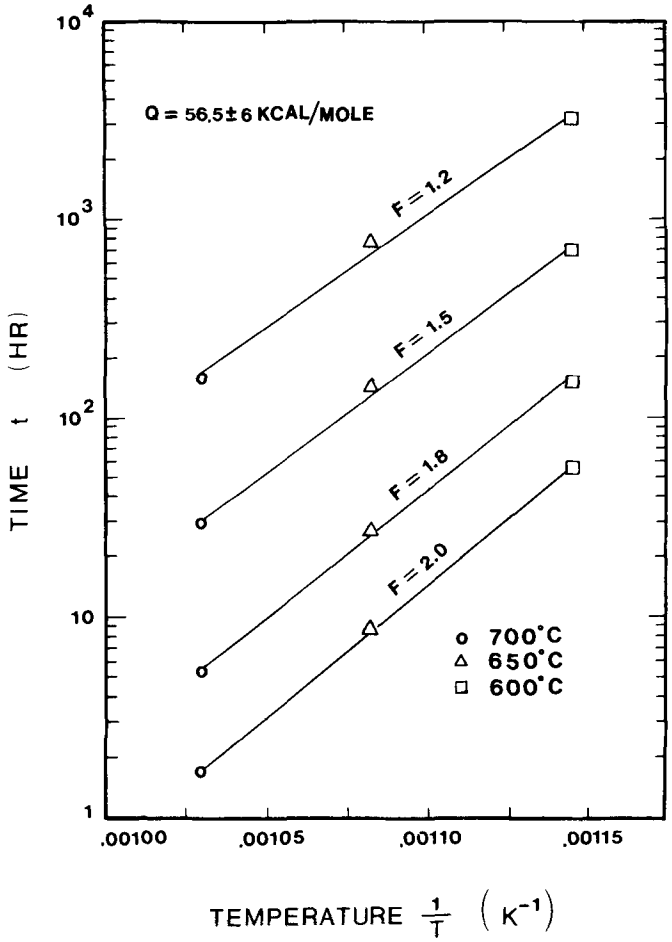

Fig. 10—Plot of log t *vs* $1/T$ for fine Fe-C alloy.

Table III. Published Data of Activation Energy Q for Iron and Carbon Diffusion

System	Q kcal/mole	References
Volume diffusion of Fe in Fe	60.7 64.0	James and Leak (1965)[30] C. Leymonie (1959)[31]
Grain boundary diffusion of Fe	41.5 40	James and Leak (1965)[29] C. Leymonie (1959)[31]
Volume diffusion of C in Fe	19.2 20.1	Honeycombe's book[33] C. Wert (1950)[32]

controlling mechanism is the volume diffusion of iron atoms in a ferrite matrix.

IV. QUANTITATIVE ANALYSIS OF THE KINETICS OF PEARLITE SPHEROIDIZATION

A. *The General Governing Equations for Mass Transport Processes during Spheroidization*

To describe quantitatively the kinetics of pearlite spheroidization, it is necessary to establish the governing diffusion equations to analyze the mass transport processes during spheroidization. Several assumptions are made, as follows:

(1) The volume fractions of each phase are conserved.
(2) The interfacial energy is isotropic. This may not be a good assumption but is a necessary one in order to simplify the mathematical analysis.
(3) The diffusion processes are carried out under the equilibrium state.

It is known from the model of fault migration theory[13,14] that the driving force for the instability of the lamellar structures is the chemical potential gradient between the highly curved lamellar faults and the flat part of interfaces. Quantitatively, the variation of the chemical potential with the curvature of the interface κ is given by the Gibbs-Thomson relation:

$$\mu = \mu_0 + \gamma\Omega\kappa\,, \qquad [18]$$

where μ_0 is the chemical potential at a flat interface, γ is the interfacial energy which is assumed to be independent of orientation, Ω is the atomic volume of the diffusing atom, and κ is the interface curvature given by:

$$\kappa = \frac{1}{R_1} + \frac{1}{R_2}$$

where R_1 and R_2 are principal radii of curvature at the interface point under consideration.

Due to the chemical potential gradient, atoms will move from the higher curvature areas to the lower curvature areas. The drift velocity of the atoms, V, is given by

$$V = -M\nabla\mu\,, \qquad [19]$$

where M is the mobility of the atoms given by

$$M = \frac{D_V\gamma\Omega}{RT}\,. \qquad [20]$$

D_V is the volume diffusivity. [D_S (interfacial diffusivity) could be used in this equation if interface diffusion was predominant.]

The volume flux, J, related to the dissolution of the fault tips and the thickening of the neighboring flat interfaces, can be expressed as:

$$J = VC_0\,, \qquad [21]$$

where C_0 is concentration of diffusing atoms. Substituting Eq. [19] and Eq. [20] into Eq. [21] yields:

$$J = -\frac{D_V C_0\gamma\Omega}{RT}\nabla\mu\,. \qquad [22]$$

When transport takes place by volume diffusion in the matrix phase under equilibrium condition, $\partial\mu/\partial t$ is negligible at any point, and therefore Laplace's equation can be utilized to describe the chemical potential field throughout the solid:

$$\nabla^2\mu = 0\,. \qquad [23]$$

The rate of the normal migration of the lamellar fault is given by

$$\frac{\partial n}{\partial t} = -\Omega J = B\nabla\mu\,, \qquad [24]$$

where

$$B = \frac{D_V C_0 \gamma \Omega^2}{RT}. \qquad [25]$$

Equation [18], Eq. [23], and Eq. [24] can be considered as the general equations governing the main diffusion process during spheroidization.

B. *Theoretical Analysis of the Migration Rate of Lamellar Faults*

Following the approach given by Nakagawa *et al.*,[34] we attempt to solve Eq. [23] by introducing a ln cosh coordinate system to describe the lamellar structure. This η-ψ coordinate system used throughout our analysis is shown in Figure 11. The transformation to the orthogonal X-Y coordinates from η-ψ is given by:[35]

$$x = \frac{a}{\pi} \ln[\cosh^2 \eta - \sin^2\psi],$$

$$y = \frac{2a}{\pi} \tan^{-1}[\tanh \eta \cdot \tan \psi] \qquad [26]$$

where a is the interlamellar spacing (see Figure 11). In the η-ψ system, Laplace's equation becomes:

$$\frac{\partial^2 \mu}{\partial \eta^2} + \frac{\partial^2 \mu}{\partial \psi^2} = 0. \qquad [27]$$

In most of the previous investigations, the geometrical shape of the lamellar termination was commonly assumed as a semicircular cap. Such a semicircular cap seems to be an unreasonable shape as it implies a discontinuous change in the interfacial curvature. In this study a curve with smoothly varying curvature, as shown in Figure 11, is introduced to represent the geometrical shape of the lamellar termination. This smoothed curve seems to be much closer to the real shape of the lamellar termination.

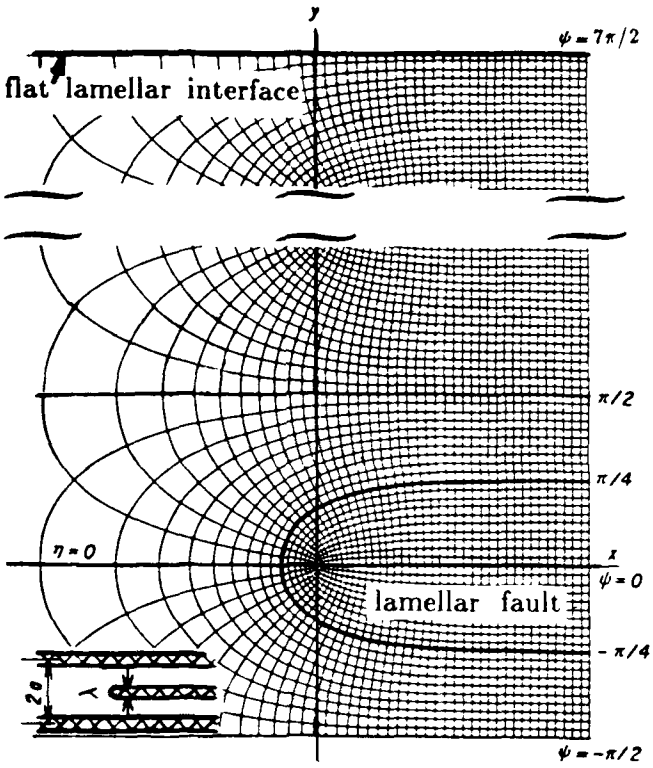

Fig. 11—The ln cosh (η-ψ) coordinates system. The lamellar fault is represented by the curve $\psi = \pi/4$ and the continuous lamellae here lie at $\psi = \pm 7\pi/2$. A model of lamellar fault is shown in the insert.

In the η-ψ coordinate system, a lamellar termination is assumed to be represented by a smoothed curve of constant ψ ($\psi = \pi/4$, as shown in Figure 11). The neighboring flat lamellae can be represented by one of the curves $\psi = \pi/2$, $3\pi/2, \ldots$ *etc.*, depending on the volume fraction of the lamellar phase. For pearlite, the volume fraction of cementite is about 0.13. Hence the corresponding position of the flat lamellae is taken at $\psi = 7\pi/2$ as shown in Figure 11. The boundary conditions for Laplace's equation thus are:

$$(1) \quad \mu = \mu_0 + \gamma\Omega\kappa(\eta, t) \quad \text{at } \psi = \pi/4,$$

$$(2) \quad \mu = \mu_0 \quad \text{at } \psi = 7\pi/2. \qquad [28]$$

In the boundary condition (2), we assume that the curvature everywhere at the flat lamellar interface remains negligibly different from zero.

The solution of Eq. [27], subject to these two boundary conditions above, is

$$\mu = \mu_0 + \gamma\Omega \int_0^\infty \left[\frac{\pi}{2a \cosh(\pi u/4)} + \frac{\pi^2 u^2 g(u)}{8a^2}\right] \cdot \frac{\sinh(7\pi/2 - \psi)u}{\sinh(13\pi/4)u} \cos u\eta \, du. \qquad [29]$$

Following a similar analysis given by Nakagawa *et al.*,[34] the migration rate of the fault tips is given by:

$$\left.\frac{\partial n}{\partial t}\right|_{\psi=\pi/4} = -\frac{\pi^2 B}{4\sqrt{2}a^2} \int_0^\infty \frac{\exp[-Bw^3u^3 \coth(13\pi u/4)t]u}{\cosh(\pi u/4)} du \qquad [30]$$

and the initial velocity at $t = 0$ is

$$\frac{\partial n}{\partial t} = \frac{\pi^2 B}{4\sqrt{2}a^2} \int_0^\infty \frac{u \coth(13\pi u/4)}{\cosh(\pi u/4)} du. \qquad [31]$$

Setting

$$K = \frac{\pi^2 B}{4\sqrt{2}} \int_0^\infty \frac{u \coth(13\pi u/4)}{\cosh(\pi u/4)} du. \qquad [32]$$

Finally, Eq. [31] becomes

$$\frac{\partial n}{\partial t} = \frac{K}{a^2} \qquad [33]$$

which tells us that the rate of fault migration is inversely proportional to the square of the interlamellar spacing, a.

C. *Quantitative Analysis of the Kinetics of Pearlite Spheroidization*

In the previous section, we derived an expression—Eq. [33]—for the migration rate of a single cementite platelet tip. Now we are looking for a general expression for the kinetics of the shape change in the entire lamellar structure. Figure 12 shows a pearlite microstructure which consists of an array of flat and faulted lamellae in which the lamellar faults are assumed to be randomly distributed throughout the structure. The volume fraction of lamellar cementite, V_l, which is equivalent to the area fraction of cementite, A_A,

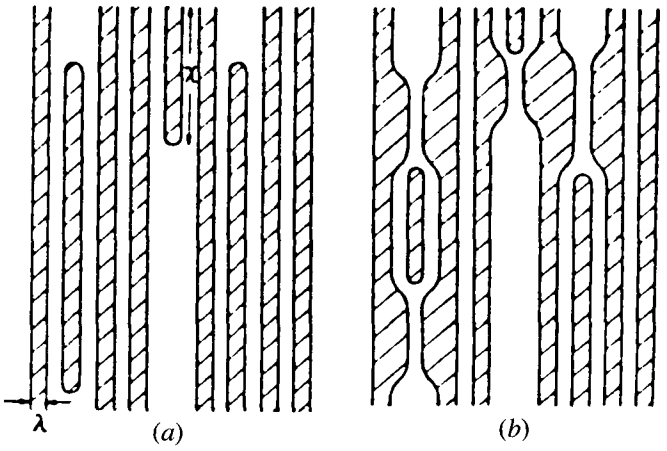

Fig. 12 — Pearlite structure consists of an array of flat and faulted lamellae: (*a*) before spheroidization, (*b*) after spheroidization.

can be given by combining Eq. [11] to Eq. [13] with Eq. [4] to Eq. [5]:

$$V_V = A_A = \frac{4}{\pi} N_A \bar{x} \bar{\lambda} , \qquad [34]$$

where $\bar{x}$ and $\bar{\lambda}$ are the average length and the average thickness of the lamellae, respectively, and N_A is the number of cementite particles in unit area.

During spheroidization, the significant geometrical changes of the lamellar cementite are the recession of the fault tips and the thickening of the lamellae.

Differentiating and rearranging Eq. [34] yields:

$$V_V \frac{d(1/\bar{\lambda})}{dt} = \frac{4}{\pi}\left(N_A \frac{d\bar{x}}{dt} + \bar{x}\frac{dN_A}{dt}\right) \qquad [35]$$

where $d\bar{x}/dt$ is the rate of the average length change of the lamellae which is equivalent to the negative value of the recession rate of the fault tip, given by:

$$d\bar{x}/dt = -\partial n/\partial t = -K/a^2. \qquad [36\text{-a}]$$

The volume fraction of cementite is related to $\bar{\lambda}$ and the interlamellar spacing, a, by

$$V_V = \bar{\lambda}/a \qquad [36\text{-b}]$$

Substituting Eq. [36-a] and Eq. [36-b] into Eq. [35] yields

$$\frac{d\bar{\lambda}}{dt} = \frac{4}{\pi} K V_V N_A - \frac{4\bar{\lambda}}{\pi V_V}(\bar{\lambda}\bar{x})\frac{dN_A}{dt}. \qquad [37]$$

Equation [37] then can be integrated to give:

$$\lambda_t - \lambda_0 = \int_{t_0}^{t}\left(\frac{4}{\pi} K V_V N_A - \frac{2V_V}{N_A S_V}\frac{dN_A}{dt}\right)dt. \qquad [38]$$

Since for a lamellar structure the lamellar thickness, $\bar{\lambda}$, is related to the specific surface area, S_V, by $\bar{\lambda} = 2V_V/S_V$, (Eq. [13]), we have, finally,

$$\left(\frac{1}{S_V}\right)_t - \left(\frac{1}{S_V}\right)_0 = \frac{2K}{\pi}\int_{t_0}^{t} N_A\, dt - \int_{(N_A)_0}^{(N_A)_t}\frac{dN_A}{N_A S_V}. \qquad [39]$$

Equation [39] can be utilized to express the kinetics of pearlite spheroidization. Quantitative evaluation of the time dependence of the reciprocal of the specific surface area, $1/S_V$, for several specimen systems of this study is accomplished by using Eq. [39]. To compare our results with theory the value of B (Eq. [25]) was taken from published experimental results.[36,37,38] From these results K could be evaluated using Eq. [32]. The values of B and K used in these calculations are shown in Table IV. Both the calculated results and the experimental results are plotted in Figures 13 to 16 for comparison.

It is seen from these figures that the theoretical analysis of the spheroidization kinetics in terms of the time dependence of reciprocal specific area, S_V, presents a reasonable agreement with the experimental results. However, it is also noted that there are some discrepancies between the theoretical and experimental curves, especially within the ranges of the final stages of the spheroidization. However, it should be realized that Eq. [39] is only an approximate expression for the kinetics because of the following:

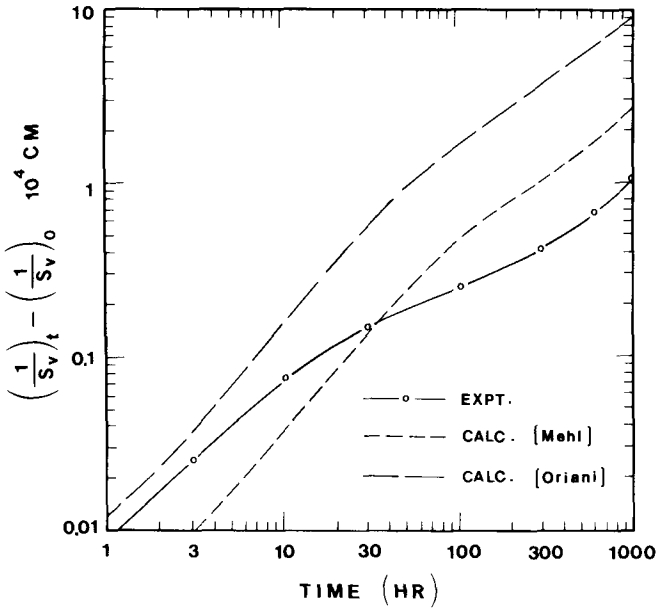

Fig. 13 — Plot of $(1/S_V)_t - (1/S_V)_0$ (coarse AISI 1080 spheroidized at 700 °C). —o— Experimental results of the present study. - - - Calculated results from Eq. [39] using the constant B given by Mehl.[36] —— Calculated results from Eq. [39] using the constant B given by Oriani.[37]

Table IV. Diffusion Constants B and K Used in the Calculation of Equation [39]

System	B, cm³/hr.	K, cm³/hr.	Reference
Commercial steel	2.63×10^{-15}	1.43×10^{-14}	Mehl[36]
	1.22×10^{-14}	6.58×10^{-14}	Oriani[37]
Fe-C alloy	5.44×10^{-14}	29.4×10^{-14}	Heckel[38]

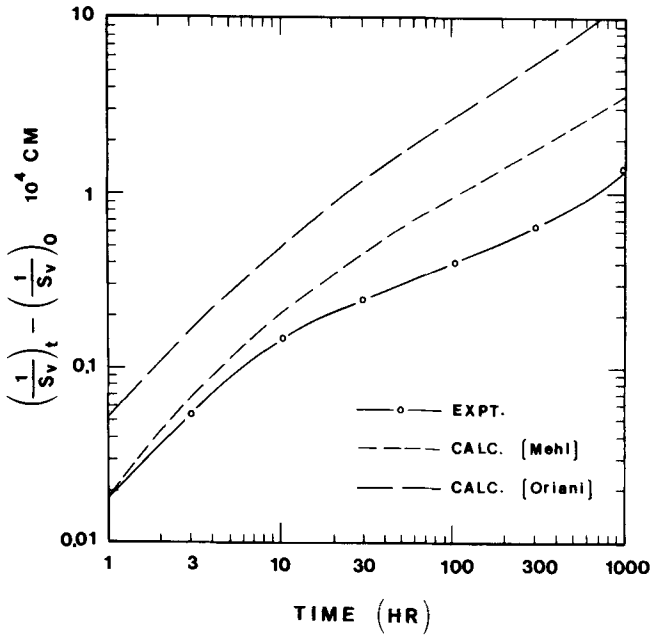

Fig. 14—Plot of $(1/S_V)_t - (1/S_V)_0$ (fine AISI 1080 spheroidized at 700 °C). —o— Experimental results of the present study. - - - Calculated results from Eq. [39] using the constant B given by Mehl.[36] —— Calculated results from Eq. [39] using the constant B given by Oriani.[37]

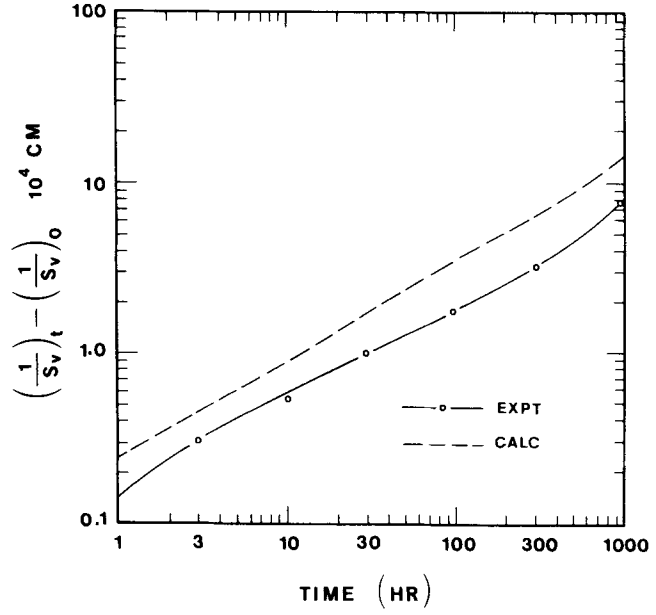

Fig. 15—Plot of $(1/S_V)_t - (1/S_V)_0$ (coarse Fe-C alloy spheroidized at 700 °C) —o— Experimental results of the present study. - - - Calculated results from Eq. [39] using the constant B given by Heckel.[38]

(1) The values of B reported in the literature vary considerably as shown in Table IV.
(2) In the later stage of spheroidization, the average shape of the structure considerably deviates from the model assumed.
(3) Subboundary groove diffusion and Rayleigh's perturbation in the early and later stages of spheroidization, respectively, were not taken into account.

From the results of the quantitative analysis presented above, it is seen that two facts play an important role in the rate of spheroidization, namely: (a) interlamellar spacing, (b) the density of faults. The reasonable agreement between the theoretical prediction and the experimental results indicated that the fault migration theory is an appropriate model for the kinetic analysis of pearlite spheroidization.

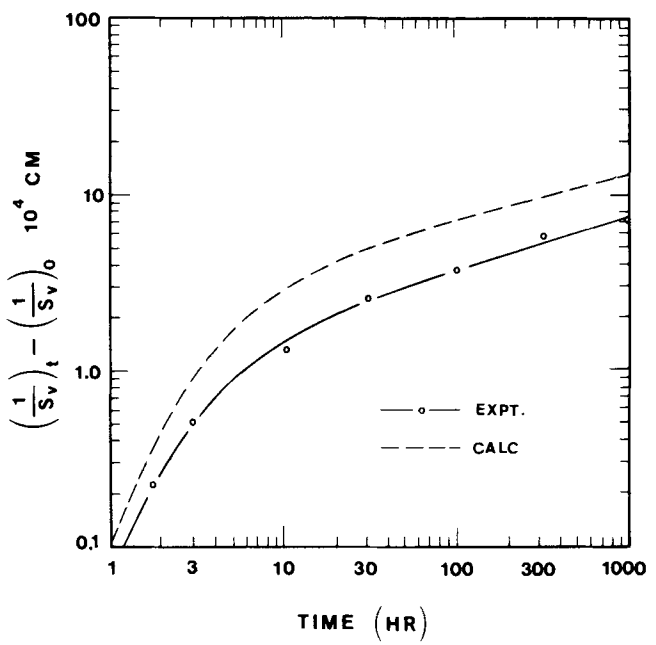

Fig. 16—Plot of $(1/S_V)_t - (1/S_V)_0$ (fine Fe-C alloy spheroidized at 700 °C). —o— Experimental results of the present study. - - - Calculated results from Eq. [39] using the constant B given by Heckel.[38]

V. CONCLUSIONS

1. A shape factor, F, defined as $F = S_V^p/3\overline{K}_m$, is a good parameter to characterize the shape evolution during spheroidization of lamellar structures. Geometrically, it represents the average aspect ratio of a lamellar structure as observed on a two-dimensional polished section.
2. In the spheroidization of undeformed pearlite, there is a linear relation between the shape factor F and the logarithm of time for a constant temperature.
3. The general rate equation in terms of the time and temperature dependence for a constant shape factor, *i.e.*, $1/t = A \exp(-Q/RT)$, is well followed. The activation energy calculated from the rate equation is interlamellar spacing independent but is composition dependent and has a value about 70 kcal/mole for AISI 1080 and about 58 kcal/mole for pure Fe-C alloy. These results indicate that the volume diffusion of Fe in ferrite is the major rate controlling mechanism.
4. Quantitative analysis based on the modified fault migration theory shows that two factors play important roles in the rate of spheroidization, namely: the interlamellar spacing and the density of faults. The theoretical predictions for the kinetics of spheroidization have a reasonable match with those of experimental result.

ACKNOWLEDGMENT

The authors express their appreciation to the reviewer of this manuscript for his helpful and insightful comments.

We have already addressed his remarks about the shape factor in the "Note Added in Proof". Here we wish to thank him for catching a mathematical error in the original manuscript and for pointing out that a mathematical simplification we had originally made was not necessary. After incorporating his suggestions relative to Eqs. [34] to [39] and recalculating the data shown in Figures 13 to 16, the agreement between theory and experiment is markedly improved.

REFERENCES

1. M. J. Harrigan and O. D. Sherby: *Mater. Sci. Eng.*, 1971, vol. 7, pp. 177-89.
2. J. Kostler: *Arch Eisenhüttenwes.*, 1975, vol. 46, pp. 229-33.
3. S. Chattopadhyay and C. M. Sellars: *Acta Metall.*, 1982, vol. 30, pp. 157-70.
4. S. Chattopadhyay and C. M. Sellars: *Metallog.*, 1977, vol. 10, pp. 89-105.
5. E. A. Chojnowski and W. J. McG. Tegart: *Metal Sci. J.*, 1968, vol. 2, pp. 14-18
6. G. W. Greenwood: *Acta Metall.*, 1956, vol. 4, pp. 243-48.
7. I. W. Lifshitz and V. V. Sloyozov: *J. Phys. Chem. Solids*, 1961, vol. 19, pp. 35-50.
8. C. Wagner: *Z. Electrochem.*, 1961, vol. 65, pp. 581-91.
9. R. T. DeHoff and C. V. Iswaran: *Metall. Trans. A*, 1982, vol. 13A, pp. 1389-95.
10. R. T. DeHoff: *Trans. AIME*, 1967, vol. 239, pp. 617-21.
11. A. M. Gokhale, C. V. Iswaran, and R. T. DeHoff: *Metall. Trans. A*, 1980, vol. 11A, pp. 1377-83.
12. R. T. DeHoff: *Acta Metall.*, 1984, vol. 43, pp. 43-47.
13. Y. L. Tian and R. W. Kraft: *Metall. Trans. A*, 1987, vol. 18A, pp. 1403-14.
14. Y. L. Tian: Ph.D. Dissertation, Lehigh University, Bethlehem, PA, 1985.
15. R. T. DeHoff and F. N. Rhines: *Quantitative Metallography*, McGraw-Hill, New York, NY, 1968.
16. E. E. Underwood: *Quantitative Stereology*, Addison-Wesley, Reading, MA, 1970.
17. E. R. Weibel: *Stereological Methods*, Acad. Pr., 1980, vol. 1.
18. H. J. C. Gundersen: *J. Microscop.*, 1977, vol. 111, pp. 219-23.
19. W. A. Mertz: *Mikroscopie*, 1967, vol. 22, p. 132.
20. E. E. Underwood: *Microscope*, 1976, vol. 24, pp. 49-64.
21. E. E. Underwood: *Proc. 4th Int. Cong. Stereology*, 1976, pp. 96-97.
22. R. T. DeHoff: *Trans. AIME*, 1964, vol. 230, pp. 764-69.
23. H. F. Fishmeister: *Z. Metallkde.*, 1974, vol. 65, pp. 558-62.
24. H. F. Fishmeister: *Powd. Met. Int.*, 1975, vol. 7, pp. 178-88.
25. A. Gallo: *Powd. Met. Int.*, 1984, vol. 16, pp. 78-80.
26. R. T. DeHoff: *Metall. Trans. A*, 1979, vol. 10A, pp. 1948-49.
27. J. H. Holloman and L. D. Jaffe: *Trans. AIME*, 1945, vol. 162, pp. 223-49.
28. F. R. Larson and J. Miller: *Trans. ASME*, 1952, pp. 765-75.
29. D. W. James and G. M. Leak: *Phil. Mag.*, 1965, vol. 12, pp. 491-503.
30. D. W. James and G. M. Leak: *Phil. Mag.*, 1966, vol. 14, pp. 701-13.
31. C. Lymonie: Ph.D. Thesis, Presented to Faculté des Science de L'Université de Paris, 1959.
32. C. A. Wert: *Phy. Rev.*, 1950, vol. 79, pp. 601-05.
33. R. W. K. Honeycombe: *Steels, Microstructure and Properties*, Edward Arnold, 1981.
34. Y. G. Nakagawa, G. C. Weatherly, and E. Ho: *Trans. JIM*, 1974, vol. 15, pp. 114-20.
35. P. Moon and D. E. Spencer: *Field Theory Handbook*, 2nd ed., Springer Verlag, 1971.
36. G. P. Airey, T. A. Hughes, and R. F. Mehl: *Trans. AIME*, 1968, vol. 242, pp. 1853-63.
37. R. A. Oriani: *Acta Metall.*, 1964, vol. 12, pp. 1399-1409.
38. K. M. Vedula and R. W. Heckel: *Metall. Trans.*, 1970, vol. 1, pp. 9-18.